Midfrequency Runout Compensation in Hard Disk Drives Via a Time-Varying Group Filtering Scheme

Chin Kwan Thum[1,2], Chunling Du[1], Ben M. Chen[2], *Fellow, IEEE*, Eng Hong Ong[1], and Kim Piew Tan[1]

[1]A*STAR Data Storage Institute, Singapore 117608

[2]Department of Electrical and Computer Engineering, National University of Singapore, Singapore 117576

Conventional add-on feedback filters that are designed to compensate for midfrequency (mid-f) repeatable runout (RRO) in a hard disk drive (HDD) servo system either have a long filter transient or constitute a large sensitivity hump as well as poor stability margins. This paper presents a novel linear time-varying (LTV) group filtering scheme for the compensation of a few mid-f RRO harmonics. While having a short filter transient that ensures fast disturbance attenuation, the proposed filter does not constitute to any substantial unnecessary sensitivity function gain amplification at the steady state. Simulation and implementation results show the effectiveness of this group filtering scheme.

***Index Terms*—Hard disk drive (HDD), linear time-varying systems, mechatronics, repeatable runout (RRO), servo systems.**

I. Introduction

INSIDE hard disk drives (HDDs), the eccentricity of the servo tracks introduces written-in repeatable runout (RRO), which is periodic and synchronized with the rotation of the disk platters. They are typically of known frequencies (generally integer multiples of the frequency of the spindle operating speed), but of uncertain phases and magnitudes. Another main source of RRO comes from the spindle motor. As RRO inside a HDD servo system can greatly degrade the HDD servo performance and thus can constitute to a lower achievable track density, the effect of RRO must be attenuated. Further, with the continuous demand for a faster data transfer rate, future HDD servo system shall not only attenuate the effect of RRO substantially, but also shortly.

As the effect of RRO can be readily shown as [1],

$$\mathrm{PES}_{\mathrm{RRO}}(t) = d_{\mathrm{RRO}}(t) * s(t) \tag{1}$$

where $\mathrm{PES}_{\mathrm{RRO}}(t)$ represents the repeatable runout that appears in the position error signal (PES), $s(t)$ is the impulse response of the sensitivity transfer function, $S(s)$, and $d_{\mathrm{RRO}}(t)$ stands for the repeatable disturbances. It is more difficult to compensate the impact of the midfrequency (mid-f) RRO that is located closely to servo bandwidth on HDD servo performance than the low-frequency (low-f) RRO as the sensitivity gain, $|S(s)|$, at the lower frequency can be significantly and easily reduced by using any classical linear control techniques. Hence, in this paper, we focus on the development a novel RRO attenuation scheme that is capable of compensating the effect of mid-f RRO substantially and quickly.

Over these years, several control feedback methods [2]–[5], [24] that are based on the internal-model-principle (IMP) [6] have been proposed to compensate the effect of RRO. From the frequency domain point-of-view, these methods typically incorporate add-on RRO compensator to deliberately insert lowly damped open loop poles at the RRO frequencies so as to create deep gain notches in $S(s)$ at the RRO frequencies. And to ensure a fast error attenuation convergence, these compensator gains have to be large such that the resultant closed loop transient characteristics of the $S(s)$ are not dominated by the lowly damped poles of the filters. Consequently, if any of those gain notches are placed at the mid-f region, i.e. close to the servo bandwidth, the width of those gain notches are usually too wide such that, under the constraints imposed by the Bode's integral theorem [7] and Bode's gain-phase relationship [7], they constitute a huge sensitivity hump that will lead to the amplification of disturbances at higher frequencies as well as poor stability margins at the steady state. On the other hand, [9] and [10] propose to use, respectively, the adaptive feedforward cancellation (AFC) method [11] and its modified version [10] to reject the effect of the RRO by injecting an adaptive feedforward signal. Accordingly, the error rejection convergence rate of the AFC scheme and its modified version are controlled by their adaptation gains. However, it is noted that the AFC system and the modified AFC system have an IMP equivalent and having large adaptation gains will also mean wide gain notches in $S(s)$ at the RRO frequencies.

In this paper, we propose a new linear time-varying (LTV) add-on RRO compensator made of a group filter to compensate for the effect of mid-f RROs. By varying the dampings and the gains of the group filter appropriately with time, our proposed RRO compensator can have a short transient that ensures a fast error convergence as well as little distortion to the basic servo performance achieved by the main feedback loop so as to avoid unnecessary disturbance amplification at higher frequencies and degradation of the stability margins at the steady state.

The outline of this paper is as follows. Section II presents our proposed LTV add-on group filter for mid-f RRO compensation with a fast error convergence rate while preserving the basic servo performance as well as the stability margins of the main feedback loop at the steady state. The design method of our proposed LTV add-on group filter is detailed in Section III. In Section IV, we will apply our proposed mid-f RRO compensation scheme to HDD servo systems. Both simulation results as

Digital Object Identifier 10.1109/TMAG.2008.2004893

Color versions of one or more of the figures in this paper are available online at http://ieeexplore.ieee.org.

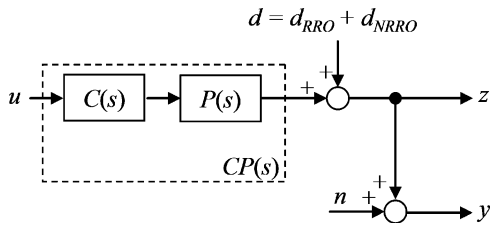

Fig. 1. Open loop block diagram of a typical HDD servo loop precompensated with a main servo compensator.

well as implementation results are presented to see how our proposed scheme fare against the conventional IMP based control scheme in both transient and steady state. Further tests to examine various other aspect of the effectiveness of our proposed method are conducted too. Lastly, we draw some concluding remarks in Section V.

II. Design of Linear Time-Varying Group Filter

In this section, we present LTV group filter for mid-f RROs compensation with parallel structure added onto the main feedback loop that is designed to provide basic servo stability and performance.

A block diagram representation of a typical HDD actuator system with disturbance injected and pre-compensated with the main servo compensator, $C(s)$, for basic servo performance and good stability in open loop is shown in Fig. 1. $P(s)$ represents the transfer function of the voice coil motor (VCM) actuator plant, which is basically made up of a double integrator with multiple resonances. z is the true PES whereas y represents the measured PES. d_{NRRO} represents the equivalent effect of all nonrepeatable runout (NRRO) disturbances, typically, torque disturbances, nonrepeatable disk and slider motions at the output channel. d_{RRO} denotes the equivalent effect of all RRO disturbances. n is measurement noise. Given that (A^{cp}, B^{cp}, C^{cp}, D^{cp}) is the matrix quadruple of $CP(s) = C(s)P(s)$, it is easily to derive from Fig. 1 that this system can be described with an equivalent continuous-time linear time-invariant (LTI) state-space representation Σ, which is given by

$$\dot{x}^{cp}(t) = Ax^{cp}(t) + B_1 w(t) + B_2 u(t) \tag{2}$$

$$y(t) = C_1 x^{cp}(t) + D_{11} w(t) + D_{12} u(t) \tag{3}$$

$$z(t) = C_2 x^{cp}(t) + D_{21} w(t) + D_{22} u(t) \tag{4}$$

with

$$A = A^{cp}, B_1 = 0, B_2 = B^{cp}, C_1 = C^{cp}, D_{11} = [1\ 0],$$
$$D_{12} = D^{cp}, C_2 = C^{cp}, D_{21} = [1\ 1], D_{22} = D^{cp}$$

where $x(t)$, $u(t)$, $y(t)$ and $z(t)$ are, respectively, the states of the pre-compensated plant, $CP(s)$, control input, measurement output and controlled output, $w(t) = [d\ n]'$. Without loss of generality, $D^{cp} = 0$.

A. Group Filter Structure: Parallel Realization

For designing convenience, the proposed LTV group filter, F_t, is added onto the main feedback loop via parallel realization, as shown in Fig. 2. It has been shown that by adopting such a

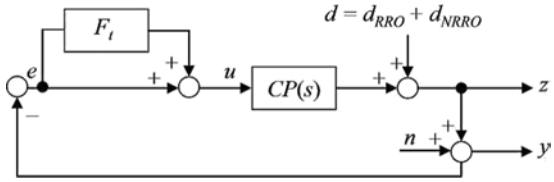

Fig. 2. Block diagram of the proposed LTV group filter, F_t, added onto the main feedback loop via parallel realization.

filter structure, we can easily decouple the control design for the main servo compensator, $C(s)$, and the proposed F_t into two separate stages [12]. The basic servo stability and performance is provided by the main feedback loop. By an abuse of notation, the resultant sensitivity function, $S(s)$ is given by

$$S(s) = S_0(s) \cdot S_F \tag{5}$$

where

$$S_0(s) = \frac{1}{1 + CP(s)} \tag{6}$$

$$S_F = \frac{1}{1 + T_0(s) \cdot F_t} \tag{7}$$

with $T_0(s)$ being the complementary sensitivity transfer function of the main feedback loop, which is given by

$$T_0(s) = \frac{CP(s)}{1 + CP(s)}. \tag{8}$$

Motivated by [12], in order to preserve the good stability margins of the main feedback loop as well as to achieve a smooth resultant sensitivity function curve, we propose the following LTV group filter, which is made up of n 2-order LTV subfilters and given by

$$F_t = \sum_{i=1}^{n} F_t^i \tag{9}$$

and state-space representation of the ith filter F_t^i is given by

$$\dot{x}_i^f(t) = A_i^f x_i^f(t) + B_i^f e(t) \tag{10}$$

$$u_i^f(t) = C_i^f x_i^f(t) + D_i^f e(t) \tag{11}$$

where

$$A_i^f = \begin{bmatrix} 0 & 1 \\ -w_i^2 & -2w_i\zeta_i(t) \end{bmatrix},\ B_i^f = \begin{bmatrix} 0 \\ 1 \end{bmatrix},$$
$$C_i^f = K_i(t) \begin{bmatrix} w_i^2 \sin(\varphi_i) & w_i \cos(\varphi_i) & +2w_i \sin(\varphi_i)\zeta_i(t) \end{bmatrix},$$
$$D_i^f = -K_i(t) \sin(\varphi_i)$$

where w_i is the ith mid-f RRO frequency, φ_i is the phase angle determined by

$$\varphi_i = \arg\left[T_0(jw_i)\right] \in (-\pi, \pi]. \tag{12}$$

$\zeta_i(t)$ and $K_i(t)$ represent, respectively, the time-varying damping ratio and the time-varying positive filter gain of F_t^i. For $\zeta_i(t)$:

i) $\zeta_i(t) \in \Re$;

ii) $0 \le \zeta_i^{\min} \le \zeta_i(t) \le \zeta_i^{\max} \le 1\ \forall t$;
iii) $0 \le |\zeta_i(t_1) - \zeta_i(t_2)| \le M_i^{\zeta}(t_1 - t_2) \forall t_1, t_2$ for some $M_i^{\zeta} > 0$ and $t_1 < t_2$.

And for $K_i(t)$:

i) $K_i(t) \in \Re$;
ii) $0 \le K_i^{\min} \le K_i(t) \le K_i^{\max}\ \forall t$;
iii) $0 \le |K_i(t_1) - K_i(t_2)| \le M_i^{K}(t_1 - t_2) \forall t_1, t_2$ for some $M_i^{K} > 0$ and $t_1 < t_2$.

Consequently, the resultant state-space representation of F_t is naturally given by

$$\dot{x}^f(t) = A^f x^f(t) + B^f e(t) \tag{13}$$
$$u^f(t) = C^f x^f(t) + D^f e(t) \tag{14}$$

where

$$A^f = diag\left\{A_1^f, A_2^f, \ldots, A_n^f\right\},$$
$$B^f = col\left\{B_1^f, B_2^f, \ldots, B_n^f\right\},$$
$$C^f = row\left\{C_1^f, C_2^f, \ldots, C_n^f\right\},\ D^f = \sum_{i=1}^{n} D_i^f.$$

The matrix quadruple of the open loop system is given by $(A_{ol}, B_{ol}, C_{ol}, D_{ol})$ where

$$A_{ol} = \begin{bmatrix} A^{cp} & B^{cp}C^f \\ 0 & A^f \end{bmatrix} \tag{15}$$
$$B_{ol} = \begin{bmatrix} (1 + D^f)' B^{cp\prime} & B^{f\prime} \end{bmatrix}' \tag{16}$$
$$C_{ol} = \begin{bmatrix} C^{cp} & D^{cp}C^f \end{bmatrix},\ D_{ol} = D^{cp}(D^f + 1). \tag{17}$$

The state representation of the resultant closed loop system can be expressed as

$$\begin{pmatrix} \dot{x}^{cp} \\ \dot{x}^f \end{pmatrix} = A_{cl} \begin{pmatrix} x^{cp} \\ x^f \end{pmatrix} \tag{18}$$

where $A_{cl} = (A_{ol} - B_{ol}C_{ol})$.

For simplicity of presentation, in the rest of this section we drop away t in $K_i(t)$ and $\zeta_i(t)$, and let $K(t)$ and $\zeta(t)$ represent, respectively, the set of K_i and ζ_i, $\forall i$.

Next, in order to prove the stability of the whole closed loop system, A_{cl} is separated into two parts, namely, the time-invariant part, A_{cl}^0, and the time-varying part, $A_\Delta(K(t), \zeta(t))$ arising from the time-varying parameters of F_t. Suppose that $(A^{cp}, B^{cp}, C^{cp}, D^{cp})$ is in controllable cannonical form with $B^{cp} = [0\ 0\ \cdots\ 1]'$. A_{cl} can then be expressed as

$$A_{cl} = A_{cl}^0 + A_\Delta\left(K(t), \zeta(t)\right) \tag{19}$$

where

$$A_{cl}^0 = \begin{bmatrix} V & 0 \\ Y & Z \end{bmatrix};$$
$$V = A^{cp} - col\{0, 0, \ldots, 0, C^{cp}\},$$
$$Y = col\{0, -C^{cp}, 0, -C^{cp}, \ldots, 0, -C^{cp}\}$$
$$Z = diag\left\{\begin{bmatrix} 0 & 1 \\ -w_1^2 & 0 \end{bmatrix}, \ldots, \begin{bmatrix} 0 & 1 \\ -w_i^2 & 0 \end{bmatrix}, \ldots, \begin{bmatrix} 0 & 1 \\ -w_n^2 & 0 \end{bmatrix}\right\}$$

and

$$A_\Delta\left(K(t), \zeta(t)\right) = A_{\Delta K} + A_{\Delta\zeta} + A_{\Delta K\zeta} \tag{20}$$

with

$$A_{\Delta K} = \begin{bmatrix} 0 & 0 \\ C^{cp} & Q \\ 0 & 0 \end{bmatrix} \begin{bmatrix} W_K^1 & 0 \\ 0 & W_K^2 \end{bmatrix},$$
$$A_{\Delta\zeta} = \begin{bmatrix} 0 & 0 \\ 0 & R \end{bmatrix} \begin{bmatrix} 0 & 0 \\ 0 & W_\zeta \end{bmatrix},$$
$$A_{\Delta K\zeta} = \begin{bmatrix} 0 & 0 \\ 0 & U \\ 0 & 0 \end{bmatrix} \begin{bmatrix} 0 & 0 \\ 0 & W_{K\zeta} \end{bmatrix}$$

where Q, R, U, W_K^1, W_K^2, W_ζ and $W_{K\zeta}$ are given by

$$-Q = row\left\{\sin(\varphi_1)w_1^2, w_1\cos(\varphi_1), \ldots, \sin(\varphi_i)w_i^2, w_i\cos(\varphi_i), \ldots, \sin(\varphi_n)w_n^2, w_n\cos(\varphi_n)\right\},$$
$$-R = diag\left\{\begin{bmatrix} 0 & 0 \\ 0 & 2w_1 \end{bmatrix}, \ldots, \begin{bmatrix} 0 & 0 \\ 0 & 2w_i \end{bmatrix}, \ldots, \begin{bmatrix} 0 & 0 \\ 0 & 2w_n \end{bmatrix}\right\},$$
$$-U = row\left\{0, 2w_1\sin(\varphi_1), \ldots, 0, 2w_i\sin(\varphi_i), \ldots, 0, 2w_n\sin(\varphi_n)\right\},$$
$$W_K^1 = -\left(\sum_{i=1}^{n} K_i \sin(\varphi_i)\right) I,$$
$$W_K^2 = diag\{K_1, K_1, \ldots, K_i, K_i, \ldots, K_n, K_n\},$$
$$W_\zeta = diag\{\zeta_1, 0, \ldots, \zeta_i, 0, \ldots, \zeta_n, 0\},$$
$$W_{K\zeta} = diag\{0, K_1\zeta_1, \ldots, 0, K_i\zeta_i, \ldots, 0, K_n\zeta_n\}.$$

Note that since $K(t)$ and $\zeta(t)$ are made up of bounded scalar functions

$$\left\|A_\Delta\left(K(t), \zeta(t)\right)\right\| < h, \quad \forall t \tag{21}$$

where h is some bounded positive constant.

Theorem 1: Given that $A_\Delta(K(t), \zeta(t)) \to A_\Delta^\infty$ as $t \to \infty$, where A_Δ^∞ is some time-invariant constant matrix, if $A_{cl}^0 + A_\Delta^\infty$ is asymptotically stable, then the origin of (18) is exponentially stable.

The following lemma is used to prove *Theorem 1*. Its proof is given in *Lemma 2.2* in [13].

Lemma 1: Let A_x be an asymptotically stable matrix and $\int_{t_0}^{\infty} \|B_x(t)\| \le b_x < \infty$ for some positive constant b_x. Then the origin of

$$\dot{x} = \left[A_x + B_x(t)\right] x, \quad \forall t_0. \tag{22}$$

is exponentially stable.

Proof of Theorem 1: (19) can be rewritten as

$$A_{cl} = A_{cl}^0 + A_\Delta^\infty + A_\Delta\left(K(t), \zeta(t)\right) - A_\Delta^\infty. \tag{23}$$

Let

$$A_x = A_{cl}^0 + A_\Delta^\infty, \quad B_x(t) = A_\Delta\left(K(t), \zeta(t)\right) - A_\Delta^\infty. \tag{24}$$

Considering (21) and $A_\Delta(K,\zeta) \to A_\Delta^\infty$ as $t \to \infty$, it becomes obvious that $\|B_x(t)\| < g$ for some positive constant g and $\|B_x(t)\| \to 0$ as $t \to \infty$. Consequently, there exists a positive $b_x < \infty$ such that $\int_{t_0}^{\infty} \|B_x(t)\| \le b_x$. According to Lemma 1, the proof can be completed.

Remark 1: From Theorem 1, the stability of the resultant time-varying closed loop system is essentially dependent on the asymptotic stability of the time-invariant matrix $A_{cl}^0 + A_\Delta^\infty$. Thus, given that the closed loop system at steady state has sufficient stability robustness against bounded and acceptable plant variations, the robust stability of the time-varying closed loop system will be guaranteed.

III. Selection of Filter Parameters

The design of the LTV group filter for RRO compensation is done by means of appropriate designing of its subfilters, F_t^i. Prior to the design of F_t^i, we assume that the main servo compensator, $C(s)$, has been properly designed to achieve basic servo stability and performance.

Here, we are interested in the speed of attenuation for any mid-f RRO with a center frequency of w_i, RRO_i. Generally, the transient time of any harmonic, t_s, inside a LTI closed loop system is dominantly determined by the pair of closed loop poles that is located closest to the harmonic frequency, which is given by [14]

$$t_s \approx \frac{4.6}{\zeta_p w_p} \tag{25}$$

where ζ_p and w_p stands for the damping ratio and center frequency of the closest pair of closed loop poles, respectively. In our case, without loss of generality, $w_p = w_i$. And using the well-known Q-factor rule [15] that identifies the strong association between the -3 dB bandwidth, Δw, of any gain notch in the frequency domain that centers at w_p and the damping ratio ζ_p of the pair of poles centering at w_p, which is given by

$$\Delta w = \zeta_p w_p \tag{26}$$

we can easily approximate the required -3 dB bandwidth of the resultant sensitivity gain notch at w_i for any desired value of ζ_p, which in turn, decides the transient time or the speed of RRO attenuation for RRO_i. Since the -3 dB bandwidth of the required sensitivity gain notch at w_i can be approximated by the 3 dB bandwidth of the i-th sub-filter, F_t^i, that is dominantly controlled by the filter gain, which in our case, the value of $K_i(t)$, it becomes apparent that by adjusting $K_i(t)$, we can decide the effective closed loop damping ratio, i.e., ζ_p, and so, the speed of RRO attenuation at any time t.

Our control strategy is as follows. Initially, when the effect of RRO_i is large, the 3 dB bandwidth of F_t^i shall be large, which consequently ensures a wide sensitivity gain notch at w_i and also a large ζ_p, and thus, a high speed RRO_i attenuation. This implies $K_i(t)$ should be large initially. As time passes by, the effect of RRO_i is reduced exponentially. So to avoid distortion to the basic servo performance as well as good stability margins achieved by the main servo compensator, $C(s)$, during the steady state, the -3 dB bandwidth of the resultant sensitivity gain notch at w_i should be small, meaning a small $K_i(t)$ as $t \to \infty$.

Let the required extra amount of attenuation at w_i provided by the ith subfilter during steady state be given by $|S_{f(desired)}^i(jw_i)|$. Then from (7), the steady state value of $|F_t^i(jw_i)|$ can be designed and given by

$$\left|F^i(jw_i)\right| = \left[\left|S_{f(\text{desired})}^i(jw_i)\right|^{-1} - 1\right] |T_0(jw_i)|^{-1}. \tag{27}$$

During the transient state of the RRO_i attenuation, as the value $K_i(t)$ is varying, $\zeta_i(t)$ should be varying accordingly to ensure that the value of $|F_t^i(jw_i)|$, which is important to magnitude of RRO_i attenuation, is appropriate.

Assuming $K_i(t) = q$ and $\zeta_i(t) = r$, where q and r are positive constant. The Laplace transform of F_i^t is given by

$$F_t^i(s) = q\frac{s\left[w_i\cos(\varphi_i) - \sin(\varphi_i)s\right]}{s^2 + 2rw_i s + w_i^2}. \tag{28}$$

By letting $s = jw_i$, from (28), the relationship between q, r and $|F_t^i(jw_i)|$ is derived and given by

$$r = 0.5\left|F^i(jw_i)\right|^{-1} q. \tag{29}$$

Thus, assuming $|F_t^i(jw_i)|, \forall t$ is a constant, the initial value and final value of $\zeta_i(t)$ and $K_i(t)$ can be designed based on the following two relationships:

$$\zeta_i^0 = 0.5\left|F^i(jw_i)\right|^{-1} K_i^0; \tag{30}$$

$$\zeta_i^\infty = 0.5\left|F^i(jw_i)\right|^{-1} K_i^\infty. \tag{31}$$

When $K_i(t)$ reduces too rapidly so as to quickly reduce the effective width of the gain notch, the speed of RRO_i attenuation also deteoriates quickly. And it is noted that in order to avoid a rapid deterioration in the speed of RRO_i attenuation as $K_i(t)$ reduces exponentially, it helps by either slowing the reduction rate of $K_i(t)$ or designing the effective $|S_f^i(jw_i)|$ to be appropriately lower than $|S_{f(desired)}^i(jw_i)|$ during the transient state. As a result, in order to achieve excellent attenuation performance during the transient state, $\zeta_i(t)$ and $K_i(t)$ should be designed such that

$$\zeta_i^{\min} \le \zeta_i(t) \le 0.5\left|F^i(jw_i)\right|^{-1} K_i(t) \le \zeta_i^{\max} \quad \forall t. \tag{32}$$

In this paper, $\zeta_i(t)$ and $K_i(t)$ are selected as

$$K_i(t) = K_i^\infty + \left(K_i^0 - K_i^\infty\right)\exp(-\beta_i t) \tag{33}$$

and

$$\zeta_i(t) = \zeta_i^\infty + \left(\zeta_i^0 - \zeta_i^\infty\right)\exp(-\gamma_i t) - \zeta_i^\infty \exp\left(-\lambda_i|t - \sigma_i|\right), \tag{34}$$

where β_i, γ_i, λ_i and σ_i are positive scalar tuning parameters that determine how fast $K_i(t)$ and $\zeta_i(t)$ approaches their steady state values, which in turns decides how fast the notch widths of the group filter shrink while maintaining an excellent attenuation performance during the transient state and avoiding unnecessary

disturbance amplification at higher frequencies and degradation of stability margins at the steady state.

To this end, the recommended procedure of selecting the design parameters for F_t^i is summarized as follows:

For $K_i(t)$,

1) Based on the desired transient time of RRO_i attenuation, t_s, from (25), compute the approximate value of ζ_p.
2) Calculate Δw from (26).
3) From (28), let $\zeta_i(t) = 0$, select an initial value for $K_i(t)$, i.e., K_i^0, s.t. the 3 dB bandwidth of the $F_i(t)|_{K_i(t)=K_i^0,\zeta_i(t)=0}$ is slightly larger than the value of Δw, which was found in Step 2.
4) Select a steady state value of $K_i(t)$, i.e., K_i^∞, where $0 < K_i^\infty < K_i^0$ and the 3 dB bandwidth of the $F_i(t)|_{K_i(t)=K_i^\infty,\zeta_i(t)=0}$ is much smaller s.t. the distortions of the frequency properties of closed loop system in the steady state, namely, the size of the sensitivity hump and the open loop stability margins, which are caused by F_t^i, are well acceptable.
5) Finally, design an appropriate value for β_i in (33).

Remark 2: In the above Step 3, the initial value for $K_i(t)$ is designed for any desired Δw from (28). Since the 3 dB bandwidth of F_t^i is dominantly determined by the value of $K_i(t)$, at this stage we will temporarily let $\zeta_i(t) = 0$ for convenience sake.

For $\zeta_i(t)$,

1) Based on the desired magnitude of RRO_i attenuation, $|S^i_{f(desired)}(jw_i)|$, from (27), compute the value of $|F^i(jw_i)|$.
2) With the selected value of K_i^0 and K_i^∞, using (30) and (31), calculate ζ_i^0 and ζ_i^∞.
3) Finally, design appropriate values for γ_i, λ_i and σ_i of (34) s.t. RRO attenuation transient settling time for RRO_i meets t_s.

IV. Application to a HDD Servo System

We proceed to design a mid-f RRO compensator for a hard disk drive using the above time-varying group filtering method. Simulation and implementation results will be given and compared with those of conventional LTI add-on filters.

A. Identification of the VCM Actuator Plant Model

Through experimental measurement, the frequency response of the actual VCM actuator was obtained with the output in micrometer and the input in voltage (V) and is shown in Fig. 3. A 12-order model obtained using the standard least square estimation method [19] is used to approximate the actual VCM actuator and given by

$$P(s) = \frac{2.18 \times 10^8}{s^2 + 1131s + 3.948 \times 10^5} \prod_{i=1}^{5} P_i^{\rm rm}(s) \tag{35}$$

with the five main resonance modes, $P_1^{\rm rm}(s)$, $P_2^{\rm rm}(s)$, $P_3^{\rm rm}(s)$, $P_4^{\rm rm}(s)$ and $P_5^{\rm rm}(s)$, given by

$$P_1^{\rm rm}(s) = \frac{0.9752s^2 + 490.2s + 6.16 \times 10^8}{s^2 + 992.7s + 6.16 \times 10^8} \tag{36}$$

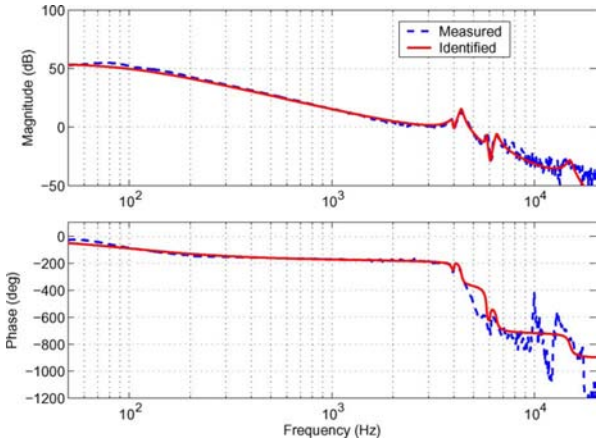

Fig. 3. Frequency response of the VCM actuator (LDV range 2 μm/V).

$$P_2^{\rm rm}(s) = \frac{0.5625s^2 - 1640s + 7.47 \times 10^8}{s^2 + 1093s + 7.47 \times 10^8} \tag{37}$$

$$P_3^{\rm rm}(s) = \frac{0.9191s^2 + 698.7s + 1.328 \times 10^9}{s^2 + 583.1s + 1.328 \times 10^9} \tag{38}$$

$$P_4^{\rm rm}(s) = \frac{0.02641s^2 - 1327s + 1.668 \times 10^9}{s^2 + 1634s + 1.668 \times 10^9} \tag{39}$$

$$P_5^{\rm rm}(s) = \frac{8.883 \times 10^9}{s^2 + 5655s + 8.883 \times 10^9}. \tag{40}$$

B. Main Servo Compensator Design

As mentioned earlier in Section II, the task of the main servo compensator, $C(s)$, is to ensure basic servo stability of the main feedback loop as well as to achieve necessary disturbance and noise rejection capability. Thus, ignoring the effect of mid-f RRO, designers may consider to design $C(s)$ in a way such that the effect of other disturbances and measurement noises is effectively attenuated to achieve high precision track-following performance. Any controller designing methods based on the advanced H_2 [16], [17] or H_∞ optimal control theory [19], [20], or even mixed H_2/H_∞ [21], [22] are highly recommended. In this paper, as we focus on the time-varying group filtering design for RROs compensation, $C(s)$ is designed as a classical PID-type controller combined with notch filters, i.e,

$$C(s) = C_{PI-Lead}(s) C_{nf}(s) \tag{41}$$

with

$$C_{PI-Lead}(s) = 6.59 \frac{s + 3302}{s} \frac{s + 6.283}{s + 2.466 \times 10^5} \tag{42}$$

and

$$C_{nf}(s) = \frac{s^2 + 1913s + 7.470 \times 10^8}{s^2 + 2.733 \times 10^4 s + 7.470 \times 10^8} \tag{43}$$

where $C_{PI-Lead}$ is a PI-Lead controller and C_{nf} is a notch filter designed to gain-stabilize the first two resonance modes located at 3.95 kHz and 4.35 kHz.

TABLE I
DESIGN SPECIFICATIONS

	700 Hz	2 kHz
1. Transient settling time (ms)	≤4	≤2
2. Extra attenuation (dB)	≥ 17	≥ 14

C. Design of the LTV Group Filter for Mid-f RRO Compensation

To evaluate the effectiveness of the proposed technique, we first assume that we have to attenuate two mid-f RROs that center at 700 Hz and 2 kHz. And the design specifications for the LTV group filter are tabulated in Table I.

Based on the given specifications, obviously,

$$w_1 = 2\pi 700\,\text{rad/s}, \quad w_2 = 2\pi 2000\,\text{rad/s}. \tag{44}$$

With the given desired settling time, using (25) and (26), the desired initial -3 dB bandwidths of the sub-filters 1 and 2 for RROs at 700 Hz and 2 kHz, are supposed to be greater than 184 Hz and 367 Hz, respectively. As a result, the initial values for $K_1(t)$ and $K_2(t)$ are chosen as

$$K_1^0 = 0.5 \text{ and } K_2^0 = 0.3. \tag{45}$$

To ensure a low sensitivity hump as well as good stability margins during the steady state, K_1^∞ and K_2^∞ are designed to be 0.15 and 0.06, such that $K_i^\infty \ll K_i^0, \forall i$. This would greatly reduce the notch widths of the proposed group filter so as to reduce the amplification of sensitivity hump as well as the degradation of the good stability margins of the resultant feedback loop at the steady state.

Consequently, to ensure attenuation factors at respective RRO frequencies as specified at the steady state, from (27), we design

$$\left|F^1(jw_1)\right| = \left|F^2(jw_2)\right| = 15\,\text{dB}. \tag{46}$$

Following (30) and (31), ζ_1^0, ζ_1^∞, ζ_2^0, ζ_2^∞ are respectively given by 0.0445, 0.0133, 0.0267 and 0.0053.

The parameters of the final group filter in the form of (9) with $n = 2$ are then given by

$$w_1 = 2\pi 700\,\text{rad/s},\ \varphi_1 = -37.0\,\text{deg}, \tag{47}$$
$$K_1(t) = 0.15 + 0.35\exp(-\beta_1 t), \tag{48}$$
$$\zeta_1(t) = 0.0133 + 0.0312\exp(-\gamma_1 t) - 0.0133\exp\left(-\lambda_1|t-\sigma_1|\right), \tag{49}$$
$$w_2 = 2\pi 1000\,\text{rad/s};\ \varphi_2 = -109.4\,\text{deg}, \tag{50}$$
$$K_2(t) = 0.06 + 0.24\exp(-\beta_2 t), \tag{51}$$
$$\zeta_2(t) = 0.0053 + 0.0214\exp(-\gamma_2 t) - 0.0053\exp\left(-\lambda_2|t-\sigma_2|\right), \tag{52}$$

and

$$\beta_1 = \beta_2 = 231, \gamma_1 = \gamma_2 = 400, \tag{53}$$
$$\lambda_1 = \lambda_2 = 105, \sigma_1 = \sigma_2 = 0.005. \tag{54}$$

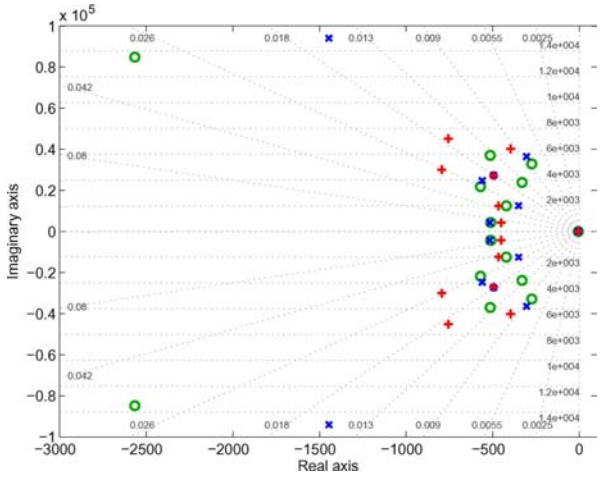

Fig. 4. Maps of eigenvalues of $A_{cl}^0 + A_\Delta^\infty$. '×': Nominal plant; '∘': Reasonances variations: -10% frequency and damping shift; '+': Reasonances variations: $+10\%$ frequency and damping shift.

D. Stability Analysis

Maps of eigenvalues of $A_{cl}^0 + A_\Delta^\infty$ for nominal plant and perturbed plants are shown in Fig. 4, where we can see that all the eigenvalues are located on the left-half plane. Hence, from *Theorem 1*, the designed LTV closed loop system is exponentially stable. Its stability is robust against $\pm 10\%$ variations in the damping and frequency of the plant resonances.

E. Simulation and Implementation Results

Prior to experiments, Matlab simulations are conducted to verify the effectiveness and performance of the proposed LTV group filtering for the RRO compensation. All controllers are discretized using the bilinear rule, except for the notch filter, $C_{nf}(s)$, which is discretized using the matched pole-zero rule, at a sampling frequency of 40 kHz. After that, experiments are conducted on a dissected HDD that is placed on a vibration free platform and its R/W head displacement is being measured with a scanning vibrometer. Controllers are implemented using a dSpace DSP installed on a desktop PC.

To compare the transient and steady state performances of the LTV feedback filtering scheme to those of the conventional LTI feedback filtering, two LTI group filters given by

$$F_{LTI1}(s) \leftrightarrow F_t|_{t=0}. \tag{55}$$

and

$$F_{LTI2}(s) \leftrightarrow F_t|_{t=\infty}. \tag{56}$$

are investigated.

Simulations based on Fig. 2 are carried out. In the simulations, 700 Hz and 2 kHz sinusoidal disturbances of any randomly picked phase angle with the amplitude of 0.4 and 0.1 μm are separately injected into the closed loop. The time traces of the respective controlled outputs using the proposed time-varying F_t, the conventional time-invariant $F_{LTI1}(z)$ and $F_{LTI2}(z)$, are shown in Fig. 5 and 6. It is seen that using either F_t or $F_{LTI1}(z)$ will meet the RRO attenuation transient

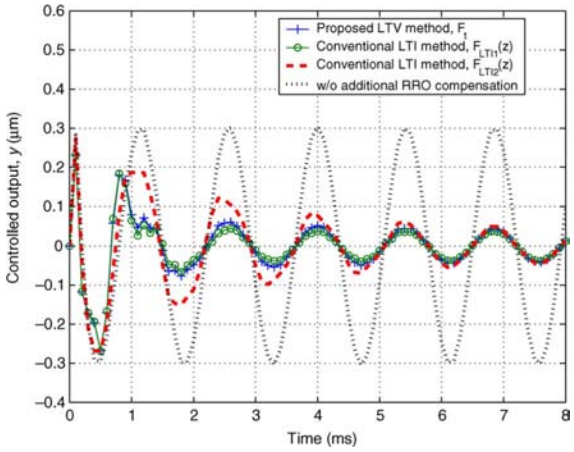

Fig. 5. Simulated disturbance responses at 700 Hz. Approx. transient settling time, F_t: 3 ms; $F_{LTI1}(z)$: 2.5 ms; $F_{LTI2}(z)$: 6.5 ms.

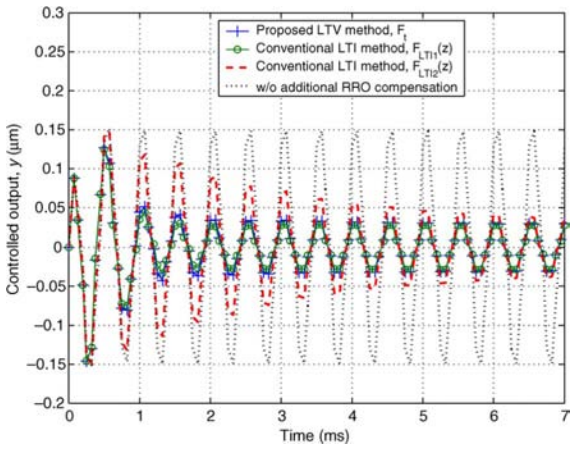

Fig. 6. Simulated disturbance responses at 2 kHz. Approx. transient settling time, F_t: 1.8 ms; $F_{LTI1}(z)$: 1.5 ms; $F_{LTI2}(z)$: 6.5 ms.

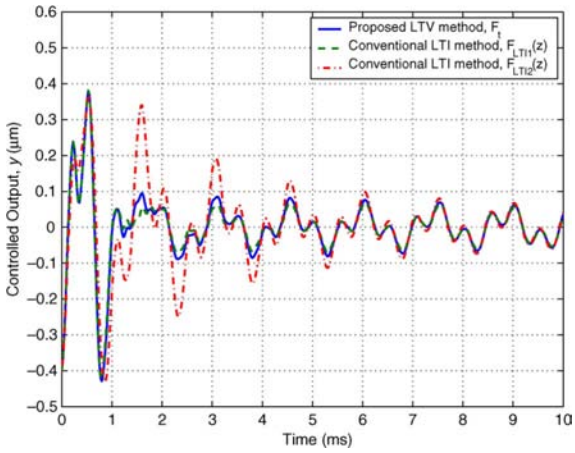

Fig. 7. Simulated combined disturbance responses at, respectively, 2 kHz and 700 Hz. Approx. transient settling time, F_t: 3 ms; $F_{LTI1}(z)$: 2.5 ms; $F_{LTI2}(z)$: 6.5 ms.

specifications, while $F_{LTI2}(z)$ will cause much slower settling. When both 700 Hz and 2 kHz sinusoidal disturbances are injected simultaneously, Fig. 7 shows that with F_t a similar settling time to that in Fig. 5 is observed.

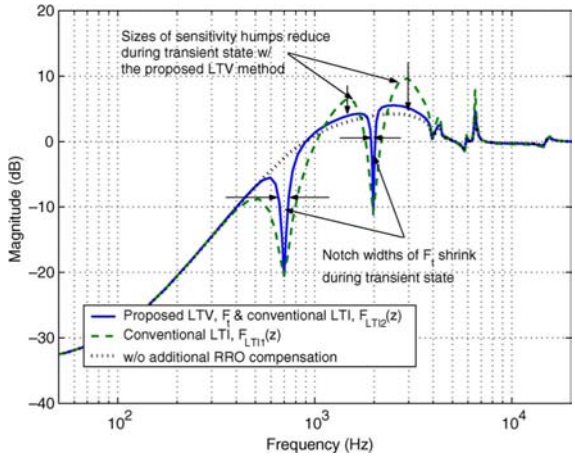

Fig. 8. Simulated sensitivity function magnitudes with respective RRO compensation scheme at the steady state. **Note: The notch widths with F_t are equally wide as those with $F_{LTI1}(z)$ and their sensitivity function humps are equally sized at $t = 0$.**

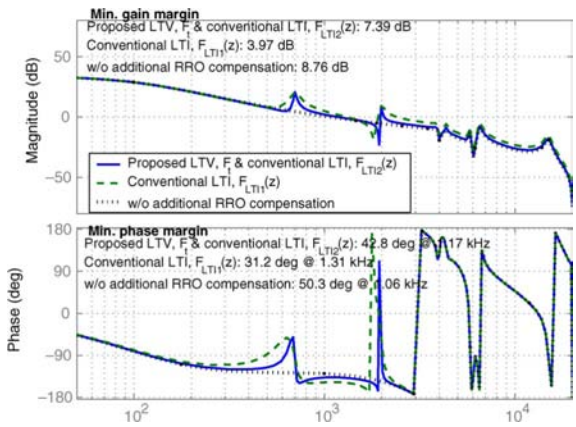

Fig. 9. Simulated open loop frequency response with respective RRO compensation scheme at the steady state.

The resultant sensitivity functions and the open loop frequency responses with respective methods are shown in Fig. 8 and 9. It is noted that while having a comparable good transient performance with the conventional $F_{LTI1}(z)$, during the steady state the proposed F_t does not display any significant degradation of the sensitivity function at higher frequencies, as seen in Fig. 8, which corresponds to a smaller amplification of high frequency disturbances. The proposed method has also managed to attain significantly higher stability margins during the steady state, and thus indicates better stability robustness as shown in Fig. 9.

During the experiments, the 700 Hz and the 2 kHz sinusoidal disturbances were separately injected into the closed loop. Similar to the simulation results, we saw that the transient responses of RRO attenuation using the proposed scheme, which are shown in Fig. 10 and 11, were very similar to those using the conventional $F_{LTI1}(z)$. The disturbance responses when both 700 Hz and 2 kHz sinusoidal disturbances are injected simultaneously is shown in Fig. 12. On the other hand, as seen in the simulation results previously, the measured transient responses of RRO attenuation were significantly more

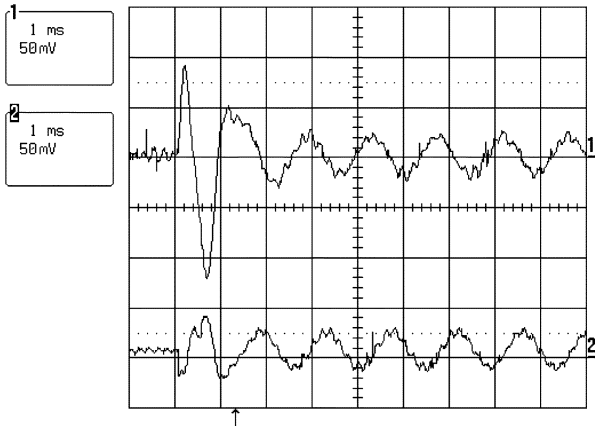

Fig. 10. Proposed LTV method, F_t: Measured disturbance responses at 700 Hz. Ch1: LDV-measurement (2 μm/V), y, Ch2: VCM-driver input, u. Approx. transient settling time: 3 ms.

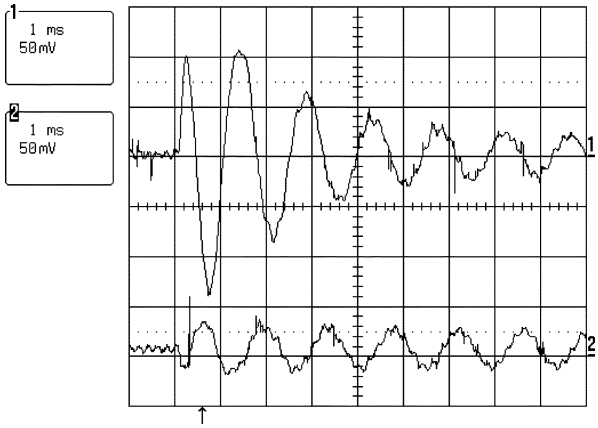

Fig. 13. Conventional LTI method, $F_{LTI2}(z)$: Measured disturbance responses at 700 Hz. Ch1: LDV-measurement (2 μm/V), y, Ch2: VCM-driver input, u. Approx. transient settling time: 7 ms.

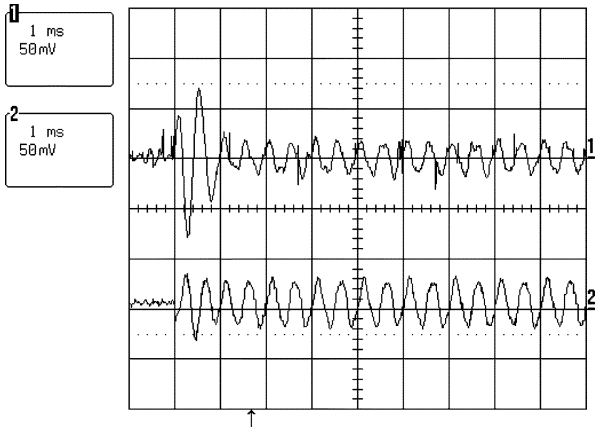

Fig. 11. Proposed LTV method, F_t: Measured disturbance responses at 2 kHz. Ch1: LDV-measurement (2 μm/V), y, Ch2: VCM-driver input, u. Approx. transient settling time: 1.5 ms.

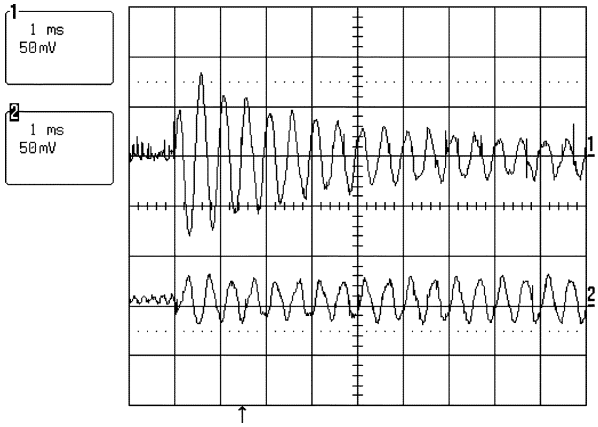

Fig. 14. Conventional LTI method, $F_{LTI2}(z)$: Measured disturbance responses at 2 kHz. Ch1: LDV-measurement (2 μm/V), y, Ch2: VCM-driver input, u. Approx. transient settling time: 6 ms.

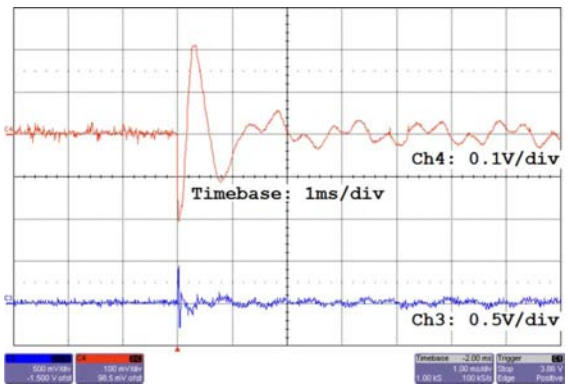

Fig. 12. Proposed LTV method, F_t: Measured disturbance responses at 700 and 2 kHz. Ch4: LDV-measurement (2 μm/V), y, Ch3: VCM-driver input, u. Approx. transient settling time: 3 ms.

oscillatory and took much longer times to settle down (133% longer for 700 Hz and 300% longer for 2 kHz), when using the conventional $F_{LTI2}(z)$, as shown in Fig. 13 and 14.

The measured sensitivity functions and the open loop bode plots are shown in Fig. 15 and 16. As displayed in Fig. 15, compared with the conventional $F_{LTI1}(z)$ which can achieve the transient RRO attenuation specifications, the proposed F_t constitutes to a significantly smaller increase in the size of the sensitivity hump in the steady state. Choosing to use the proposed F_t over the conventional $F_{LTI1}(z)$ also helps to preserve the good stability margins achieved by the main servo compensator, as shown in Fig. 16. The details are tabulated in Table II.

Remark 3: In the above application results, a 20 dB attenuation is achieved for 700 Hz RRO and a 10 dB attenuation is attained for 2 kHz RRO. A further attenuation, say 80 dB, can also be achieved by using the proposed method for 700 Hz RRO, seen in Fig. 17. The simulated disturbance responses is shown in Fig. 18. The corresponding implementation result is shown in Fig. 19. Such a high attenuation requires $\zeta_i(t)$ in (34) to operate within very small range close to zero, thus $K_i(t)$ in (33) becomes only available tuning parameter to achieve a fast transient settling time and a low sensitivity function hump at the steady state. β_i in $K_i(t)$ has to be reduced a lot, leading to a slower convergence of $K_i(t)$ and resulting in a slower reduction of sensitivity function hump to its steady state height. As for 2 kHz RRO which frequency is higher than the system bandwidth, a higher attenuation up to 80 dB is possible theoretically. However, in practical application, such a high peak threatens the

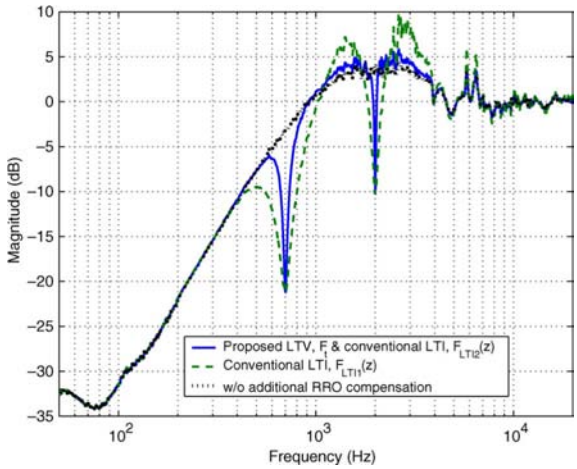

Fig. 15. Measured sensitivity functions with respective compensation scheme at the steady state.

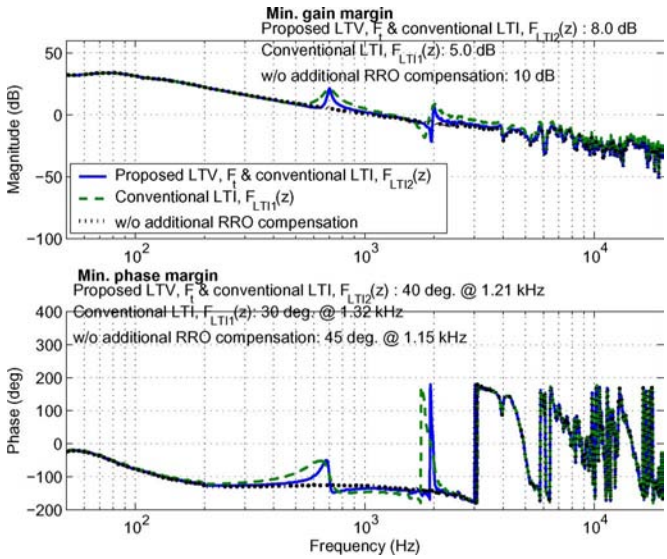

Fig. 16. Measured open loop frequency responses with respective compensation scheme at the steady state (LDV range 2 μm/V).

TABLE II
COMPARISON OF STABILITY MARGINS AT STEADY STATE

Control Scheme	Min. Gain margin (dB)	Min. Phase margin (deg.)	Open-loop Bandwidth (kHz)
w/o additional RRO compensation	10.0	45	1.15
Proposed LTV, F_t& conventional LTI, $F_{LTI2(z)}$	8.0	40	1.21
Conventional LTI, $F_{LTI1(z)}$	5.0	30	1.32

stability of the whole system under modeling error and uncertainties [3], [23].

Remark 4: According to the approximation of t_s in (25), the transient settling time is disproportionate to the damping and the frequency. This is why it is difficult to achieve a shorter settling time for 700 Hz and 2 kHz RRO compensations than those in Fig. 5 and 6. However, with a higher RRO frequency, it is possible to have a shorter settling time. Thus a filter for

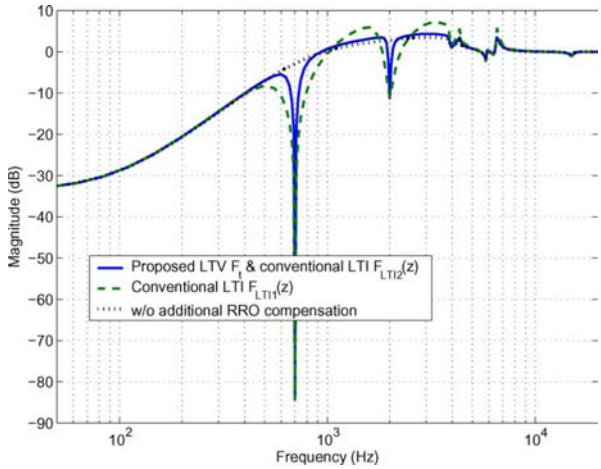

Fig. 17. Simulated sensitivity functions with respective compensation scheme at the steady state.

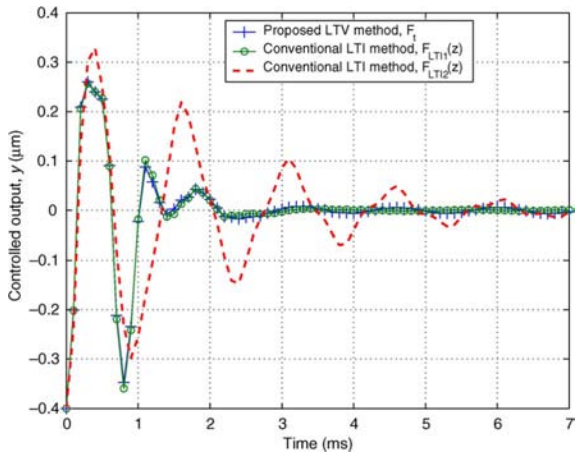

Fig. 18. Simulated disturbance responses of 0.4 μm at 700 Hz. Approx. transient settling time, F_t: 3 ms; $F_{LTI1}(z)$: 2.5 ms; $F_{LTI2}(z)$: 6.5 ms.

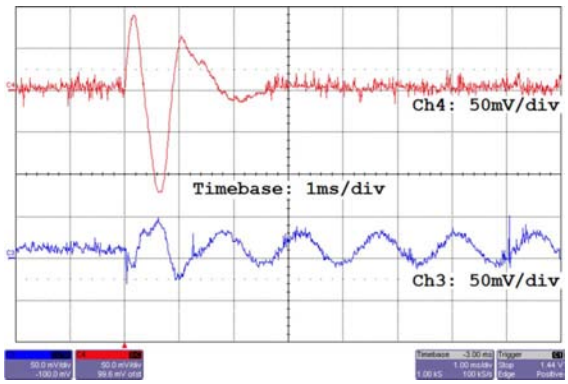

Fig. 19. Proposed LTV method, F_t: Measured disturbance responses of 0.4 μm at 700 Hz. Ch4: LDV-measurement (2 μm/V), y, Ch3: VCM-driver input, u. Approx. transient settling time: 3 ms.

3 kHz RRO compensation, F_t^3, is designed with the following parameters

$$w_3 = 2\pi 3000 \text{ rad/s};\ \varphi_3 = -148.4 \text{ deg} \tag{57}$$

$$K_3(t) = 0.06 + 0.44\exp(-\beta_3 t) \tag{58}$$

$$\zeta_3(t) = 0.0075 + 0.0553\exp(-\gamma_3 t)$$

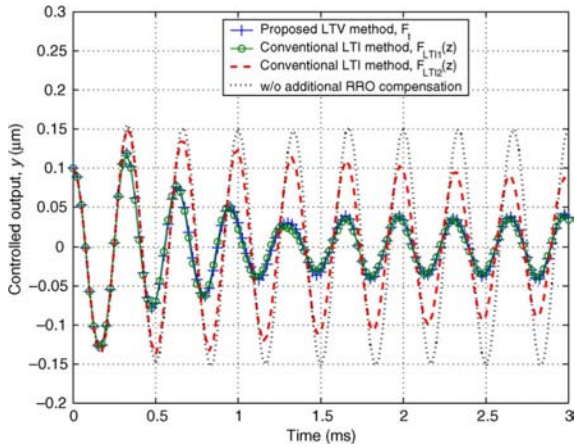

Fig. 20. Simulated disturbance responses of 0.1 μm at 3 kHz. Approx. transient settling time, F_t: 0.9 ms; $F_{LTI1}(z)$: 0.7 ms; $F_{LTI2}(z)$: 10 ms. Note: $F_t = F_t^3 + F_t^4$.

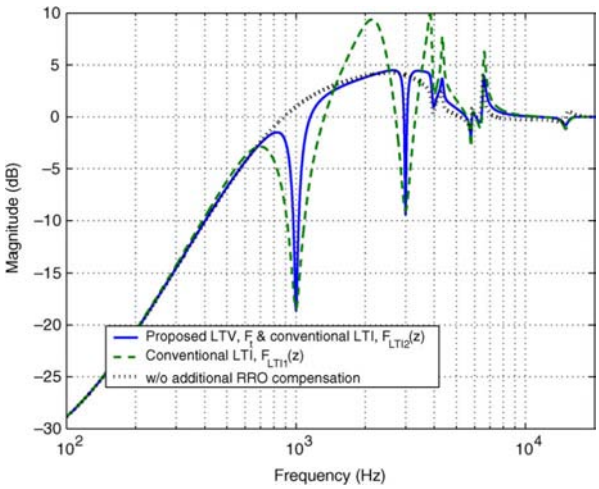

Fig. 21. Simulated sensitivity functions with respective RRO compensation scheme at the steady state. Note: $F_t = F_t^3 + F_t^4$.

$$- 0.0075 \exp(-\lambda_3 |t - \sigma_3|) \quad (59)$$

$$\beta_3 = 200,\ \gamma_3 = 300,\ \lambda_3 = 300,\ \sigma_3 = 0.002. \quad (60)$$

It turns out that a shorter settling time of 0.9 ms is achieved for 3 kHz RRO compensation, as observed in Fig. 20 and 22, and the corresponding sensitivity function is shown in Fig. 21.

Remark 5: For the RRO harmonic that is near the open-loop gain crossover frequency of the main feedback loop, say 1 kHz, the parameters of the time-varying filter, F_t^4, are designed as follows.

$$w_4 = 2\pi 1000 \text{ rad/s};\ \varphi_4 = -58.4 \text{ deg} \quad (61)$$

$$K_4(t) = 0.15 + 0.35 \exp(-\beta_4 t) \quad (62)$$

$$\zeta_4(t) = 0.00133 + 0.0311 \exp(-\gamma_4 t) - 0.0133 \exp(-\lambda_4 |t - \sigma_4|) \quad (63)$$

$$\beta_4 = 231,\ \gamma_4 = 400,\ \lambda_4 = 105,\ \sigma_4 = 0.003. \quad (64)$$

The simulated disturbance response at 1 kHz is shown in Fig. 23, with the sensitivity function plotted in Fig. 21.

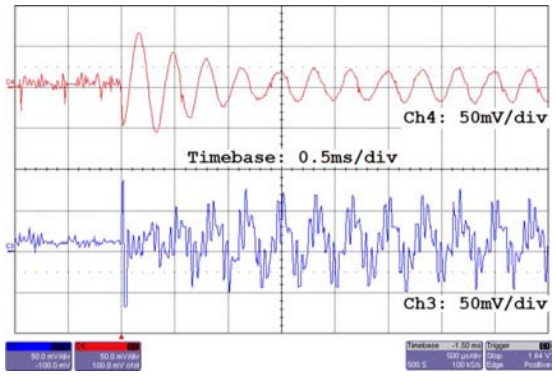

Fig. 22. Proposed LTV method, F_t: Measured disturbance responses of 0.1 μm at 3 kHz. Ch4: LDV-measurement (2 μm/V), y, Ch3: VCM-driver input, u. Approx. transient settling time: 1 ms. Note: $F_t = F_t^3 + F_t^4$.

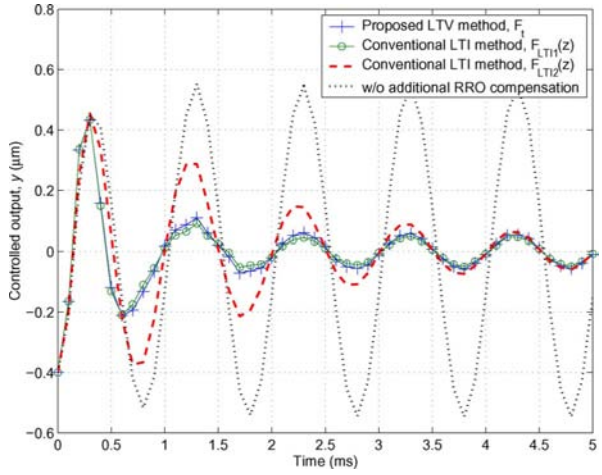

Fig. 23. Simulated disturbance responses of 0.4 μm at 1 kHz. Approx. transient settling time, F_t: 2.3 ms; $F_{LTI1}(z)$: 2 ms; $F_{LTI2}(z)$: 4 ms. Note: $F_t = F_t^3 + F_t^4$.

V. Conclusion

In this paper, a novel LTV group filtering method for a few mid-f RRO compensation has been proposed. By varying the filter gains and damping ratios exponentially with time, the proposed LTV method has shown that it can achieve good transient disturbance attenuation performance without compromising the good steady state performance as well as stability robustness. Such a result is not theoretically achievable when using any of the conventional LTI methods. Simulation and experimental results have verified the effectiveness of the proposed method in compensation for two mid-f RRO harmonics, and the comparison with the conventional LTI methods has also been made to demonstrate the benefits of the proposed LTV group filtering method. Various other aspects of the effectiveness of our proposed method have been examined too.

References

[1] Q. Jia, Z. Wang, and F. Wang, "Repeatable runout disturbance compensation with a new data collection method for hard disk drive," *IEEE Trans. Magn.*, vol. 41, no. 2, pp. 791–796, Feb. 2005.

[2] S. C. Wu and M. Tomizuka, "Repeatable runout compensation for hard disk drives using adaptive feedforward cancellation," in *Proc. Amer. Cont. Conf.*, Jun. 2006, pp. 382–387.

[3] Y. Onuki and H. Ishioka, "Compensation for repeatable tracking errors in hard drives using discrete-time repetitive controllers," *IEEE-ASME Trans. Mechatron.*, vol. 6, no. 3, pp. 132–136, Jun. 2001.
[4] C. Kempf, W. Messner, M. Tomizuka, and R. Horowitz, "A comparison of four discrete-time repetitive control algorithms," *IEEE Control Syst. Mag.*, vol. 13, pp. 48–54, Oct. 1993.
[5] L. Guo, "Reducing the manufacturing costs associated with hard disk drives-A new disturbance rejection control scheme," *IEEE-ASME Trans. Mechatron.*, vol. 2, no. 2, pp. 77–85, Jun. 1997.
[6] B. A. Francis and W. M. Wonham, "The internal model principle of control theory," *Automatica*, vol. 12, no. 5, pp. 457–465, 1976.
[7] H. Bode, *Network Analysis and Feedback Amplifier Design*. New York: D. Van Nostrand, 1945.
[8] J. Chen, "Sensitivity integrals and transformation techniques: A new perspective," *IEEE Trans. Autom. Control*, vol. 42, no. 7, pp. 1037–1044, Jul. 1997.
[9] A. H. Sacks, M. Bodson, and W. Messner, "Advanced methods for repeatable runout compensation," *IEEE Trans. Magn.*, vol. 31, no. 2, pp. 1031–1036, Mar. 1995.
[10] S. Weerasooriya, J. Zhang, and T. S. Low, "Efficient implementation of adaptive feedforward runout cancellation in a disk drive," *IEEE Trans. Magn.*, vol. 32, no. 5, pp. 3920–3922, Sep. 1996.
[11] M. Bodson, A. Sacks, and P. Khosla, "Harmonic generation in adaptive feedforward cancellation schemes," *IEEE Trans. Autom. Control*, vol. 39, no. 9, pp. 1939–1944, Sep. 1994.
[12] J. Zheng, G. Guo, Y. Wang, and W. E. Wong, "Optimal narrow-band disturbance filter for PZT-actuated head positioning control on a spin-stand," *IEEE Trans. Magn.*, vol. 42, no. 11, pp. 3745–3751, Nov. 2006.
[13] K. S. Narendra and A. M. Annaswamy, *Stable Adaptive Systems*. Mineola, NY: Dover, 2005.
[14] G. F. Franklin, J. D. Powell, and A. Emami-Naeini, *Feedback Control of Dynamic Systems*, 5th ed. Englewood Cliffs, NJ: Pearson Prentice Hall, 2006.
[15] A. Antoniou, *Digital Filters: Analysis, Design, and Applications*, 2nd ed. New York: McGraw-Hill, 1993.
[16] Z. Li, G. Guo, B. M. Chen, and T. H. Lee, "Optimal control design to achieve highest track-per-inch in hard disk drives," *J. Info. Storage Proc. Syst.*, vol. 3, pp. 27–41, Apr. 2001.
[17] J. C. Doyle, K. Glover, P. P. Khargonekar, and B. A. Francis, "State space solutions to standard H_2 and H_∞ control problems," *IEEE Trans. Autom. Control*, vol. 34, no. 8, pp. 831–847, Aug. 1989.
[18] D. Liberzon, *Switching in Systems and Control*. Cambridge, MA: Birkhäuser, 2003.
[19] B. M. Chen, T. H. Lee, K. Peng, and V. Venkataramanan, *Hard Disk Drive Servo Systems*, 2nd ed. New York: Springer, 2006.
[20] K. Zhou, J. C. Doyle, and K. Glover, *Robust and Optimal Control*. Englewood Cliffs, NJ: Pearson Prentice Hall, 1996.
[21] P. P. Khargonekar and M. A. Rotea, "Mixed H_2/H_∞ control: A convex optimization approach," *IEEE Trans. Autom. Control*, vol. 36, no. 7, pp. 824–837, Jul. 1991.
[22] C. Du, L. Xie, J. N. Teoh, and G. Guo, "An improved mixed H_2/H_∞ control design for hard disk drives," *IEEE Trans. Control Syst. Technol.*, vol. 13, no. 5, pp. 832–839, Sep. 2005.
[23] N. O. P. Arancibia, C.-Y. Lin, T.-C. Tsao, and J. S. Gibson, "Adaptive-repetitive control of a hard disk drive," in *Proc. IEEE Conf. CDC*, New Orleans, LA, Dec. 12–14, 2007, pp. 4519–4524.
[24] C. Duan, G. Guo, C. Du, and T. C. Chong, "Robust compensation of periodic disturbances by multirate control," *IEEE Trans. Magn.*, vol. 44, no. 3, pp. 413–418, Mar. 2008.

Manuscript received September 27, 2007; revised August 19, 2008. Current version published January 08, 2009. Corresponding author: C. K. Thum (e-mail: ckthum@nus.edu.sg).